HAWT report for Design of Fluid Machines for Clean Power Generation 2018

Baio Luigi
Gussoni Enrico
Ierardi Cristian
Mezzanotte Alberto

June 16, 2018

Contents

Chapter 1

Introduction

As part of the master course of Design of Fluid Machine for Clean Power Generation we were asked, divided in groups of four among energetic and mechanical engineers, to study the preliminary design of an *horizontal axis wind turbine* (**HAWT**). Requirements for this work were:

- to choose location and design condition of our machine
- to study the aerodynamics at design condition
- to make an off-design assessment
- to provide an "original part" about another topic of interest in the HAWT field

Our group was made by two mechanical engineers (Enrico and Luigi) and two energetic engineers (Alberto and Cristian) from Politecnico di Milano.

Chapter 2

Initial data

The first decision we had to take was the installation place of the machine. We started evaluating wind availability in our country, Italy, looking at data from RSE Atlante Eolico database[1]. We discovered that one of the most windy places in Italy is the island of Pantelleria with an average wind speed of 9 m/s between 75 and 100 m $a.s.l.$ as can be seen in figure 2.1. So we decided to use this as design condition.

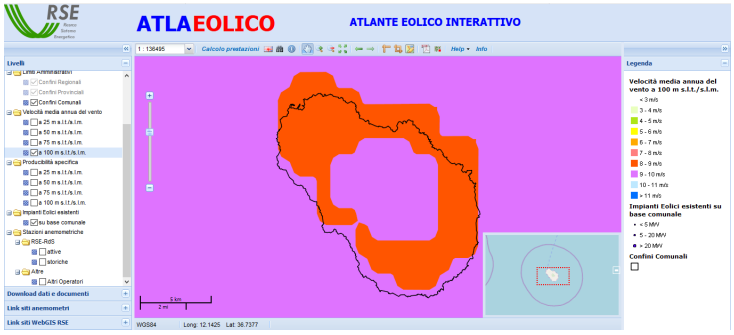

Figure 2.1: Wind distribution in Pantelleria at 100 m a.s.l.

The 80 km^2 island has more than 7700 inhabitants and shares with almost all other small Italian islands the problem of energetic sustainability. In fact in those contexts electric energy is mainly produced with diesel generators working with fuel that has to be transported by ship from the continent.
We discovered that a preliminary project for a wind-generator in Pantelleria is under development right now. The problem has been investigated in detail

[1] http://atlanteeolico.rse-web.it/

also for the specific case of Pantelleria [2] [3] [4] and the location has been defined "*favorable to the development of wind power plants of any type or size*"[5].
The specific position should be better investigated considering many parameters like the visual impact (very important in a community that mainly lives of tourism) and acoustic impact. However there is already an airport in the north-est part of the island causing problems of noise.
A simulation of visual impact which keeps in consideration the morphology of the island is represented in figure 2.2.

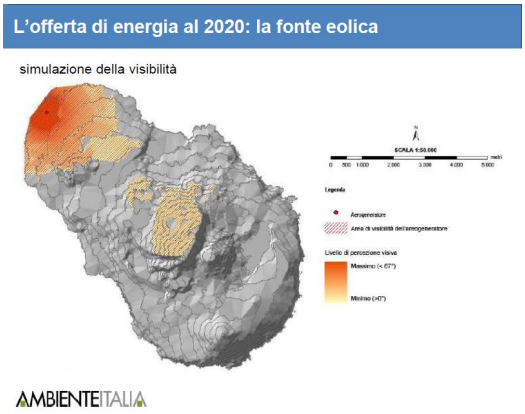

Figure 2.2: Simulation of visual impact for an HAWT in Pantelleria

For what concerns ours task we were asked to study a turbine with a rotor diameter of 68,5 m to extract as much power as possible. We choose the three-bladed option because it is by far the most commonly used in Europe (and in Italy) also considering the imposed size of the machine.
To simplify our analysis the *Tip-Speed Ratio* (**TSR**) λ, that is the ratio between the velocity of the blade tip and the velocity of the wind, was considered fixed and equal to $\lambda = 7$. This is because statistical analysis have shown that most of the three-bladed HAWT reach optimum performances (in terms of the *power coefficient* C_p) around this value.

[2] Il sistema energetico dell'isola di Pantelleria, Rodolfo Pasinetti
[3] ENEA – Rinnovabili e smart grid per le isole minori, Gian Piero Celata
[4] Piano d'azione per l'energia sostenibile, Comune di Pantelleria
[5] Pantelleria Isola Eenergica -Terra, Mare, Sole e Vento – Scenari di un futuro sostenibile, Rodolfo Pasinetti for AmbienteItalia

Chapter 3

Design condition

3.1 Aerodynamic model

Preliminary design of HAWT, given their huge dimension and aerodynamical complexity, is still studied with the two-dimensional Blade Element Momentum (BEM) theory developed by Glauert in the '30s. First of all the three blades are considered independent one from the others (that in reality is not true, also considering big size machine, but is anyway a good approximation). Than the aerodynamic performances of the blade are evaluated only at some positions along the radial coordinate (where section's profile is chosen) and than they are interpolated all along the blade span. The very first choice is the one for the profiles to be used at the *hub* of the blade, at the *tip* and at midway between them (*primary*).
Since the design of the part connecting the blade to the ogive of the nacelle is designed considering structural loads we considered the *hub radius* (r_H) at 20% of the blade radius. Than, because of the complex geometry of real blade tips and the vortex detachment that occurs there (that is nothing but two dimensional), we fixed the *tip radius* at 96% of the blade radius. By consequence, the primary was at 70% of the radius.
To choose aerodynamic profiles for this locations we based our selection on "airfoil families"[1] proposed by the *National Renewable Energy Laboratory* (**NREL**) for machines with a rotor diameter larger than $40m$. These three profiles were the NREL S818 for the hub, the NREL S827 for the primary and the NREL S828 for the tip.
As can be seen in figure 3.1 the S818 profile has a *drag coefficient* (C_d) very low and almost constant in the common operational range of the *attack angle* (α) while the *lift coefficient* (C_l) has a linear behaviour before the start of

[1] http://wind.nrel.gov/airfoils/AirfoilFamilies.html

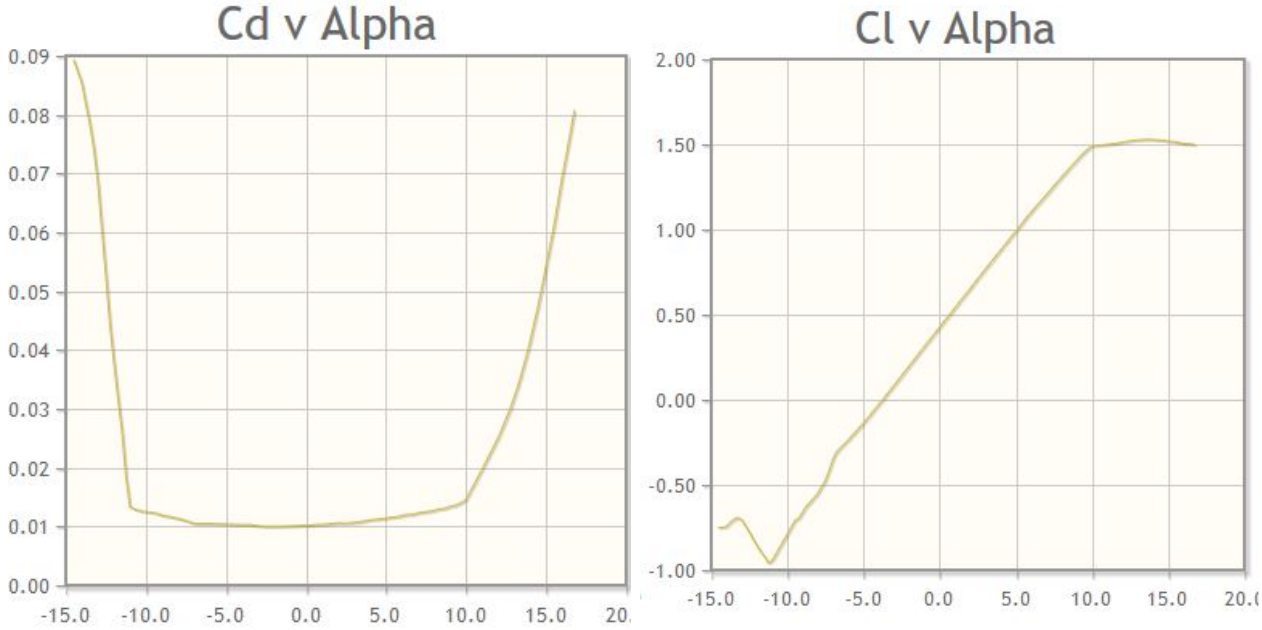

Figure 3.1: C_l (*right*) and C_d (*left*) coefficient for NREL S818 as a function of the attack angle

the stall condition and after that remains almost constant. This is a very good condition from the point of view of control and aerodynamic stability of the profile (and so of the blade).
The situation is quite different for S827 (figure 3.2) and S828 (figure 3.3) profiles where the C_l curve has a double peak before the stall and than a decrease.

Considering that we were not asked to do a "try and error" optimization of the profiles choice, the next step has been to build a database with data for each profile. This means to collect experimental data for the variation of C_l and C_d with α and the *Reynolds number* (**Re**). We faced the problem that on NREL website there are data[2] available also for high Re but for a relatively small amount of angles, while on the Airfoiltools[3] database the range of data is better but they are available only for Re$< 10^6$. This is a problem considering that in the study of large-sized wind turbines Re can reach values up to $5 * 10^6$ or more.
We had to interpolate available data to create a suitable set for our calculations. At first we developed and run the code on the range $-4° < \alpha < 16°$

[2]http://wind.nrel.gov/airfoils/Coefficients
[3]http://airfoiltools.com

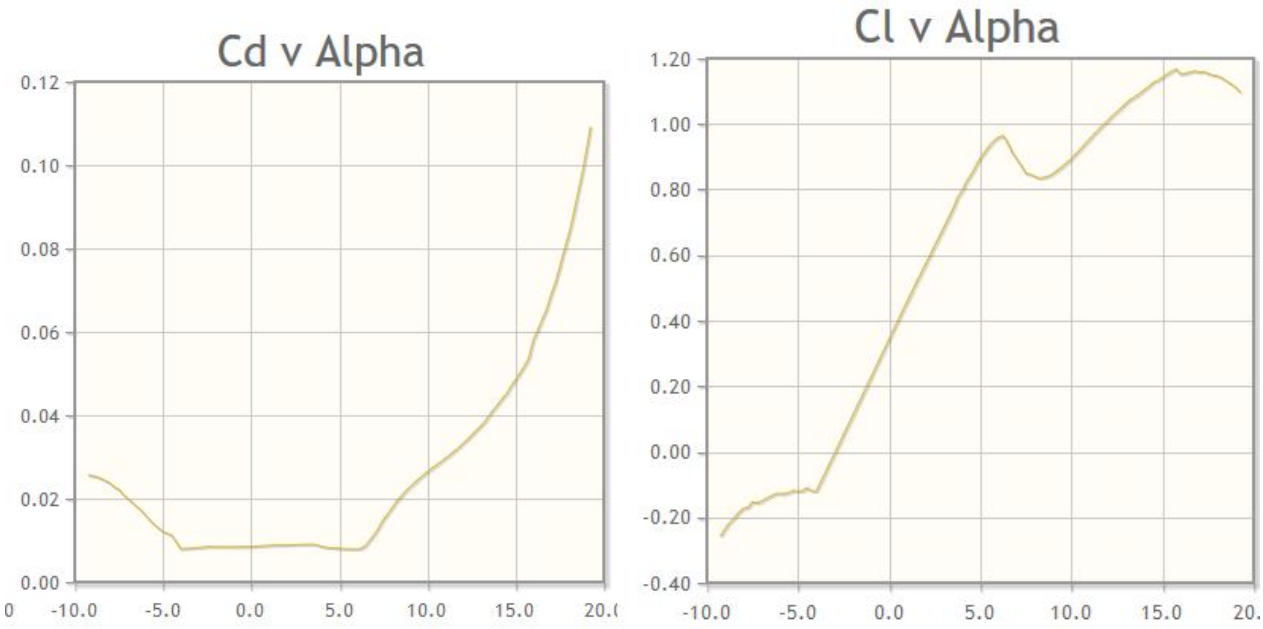

Figure 3.2: C_l (*right*) and C_d (*left*) coefficient for NREL S827 as a function of the attack angle

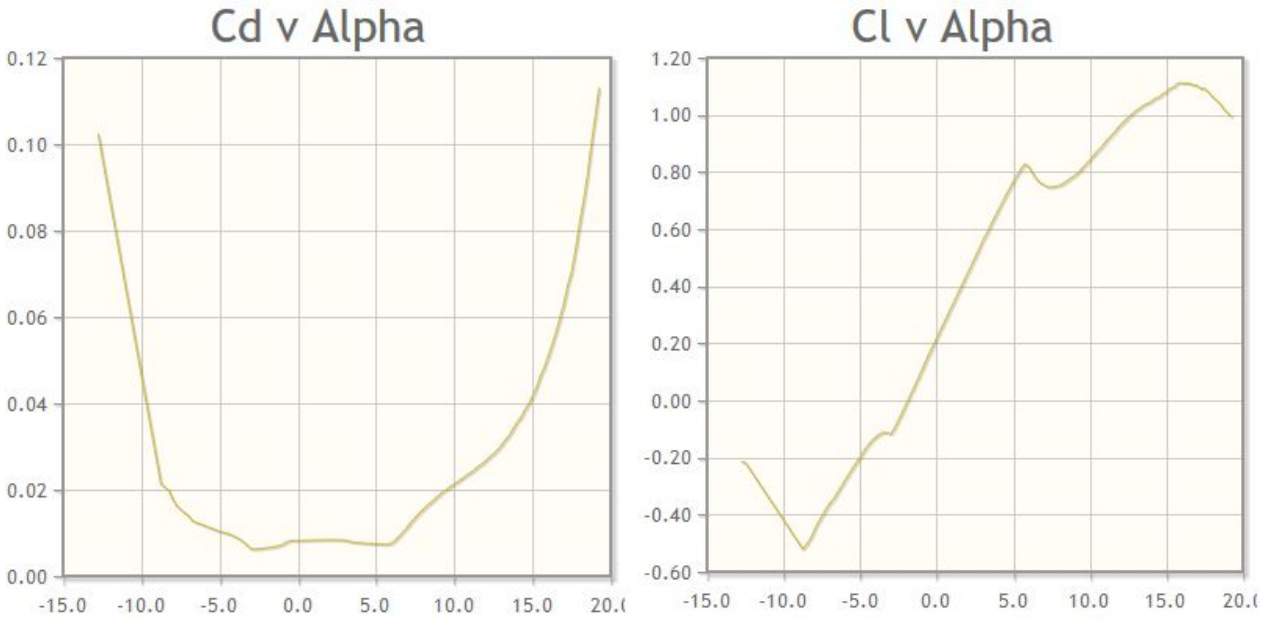

Figure 3.3: C_l (*right*) and C_d (*left*) coefficient for NREL S828 as a function of the attack angle

using Airfoiltools data for Re= 10^6. Afterwards we interpolated on the same interval data from NREL for Re up to $3.5 * 10^6$ and we found a difference in the final evaluated power around the 0.1%. We have also to consider the worst interpolation that is done in this case because of data quality.

3.2 BEM algorithm

First of all we have to solve the aerodynamic problem for each reference profiles. Without going deeply in the aerodynamic details of wings and blades we have to spend some words about the Glauert model to consider three dimensional effects in the two dimensional model. Provide that the Mach number of the flow is very low (for sure M< 0.3) the incoming flux is affected by the presence of the turbine so that the effective angle of attack and absolute speed near the blade will be different from the reference "*undisturbed*" one.
As reported in Figure 3.4 two coefficients are defined: a, to quantify the axial speed reduction and a' for the tangential variation. Both are caused by enlargement of the stream-tube upstream of the rotor. The two coefficients have to be evaluated experimentally and their values are reported in tables as function of $x = \omega * r/(V_0)$. The relation between a and a' is reported in (3.1).

$$a' = (1 - 3a)/(4a - 1) \tag{3.1}$$

Gauert model is better if compared to the Betz's one however too simple to model some important effects: it still considers an *actuator disk* (**AD**) with infinite blades, no drag (resistance) is considered and neglect the radial deviation of the flow brings to non-physical values for $\alpha < 0.5$, where α is $1-a$, and can be seen as a volumetric efficiency of the machine. Some experimental correlations have been investigated for other values of the induction factor, as can be seen in Figure 3.5.

Another important correction to do is the one proposed by Prandtl to keep in consideration the momentum effect produced by vortex detachment from the tip of each blade. This has to be considered while moving from the AD model to one with a finite number of blades. After an honourable mathematical effort, the physical effect can be modelled by multiply the torque equation by a coefficient F as shown in equation (3.2) and after.

$$dt = F4\pi r dr \rho V_0 2a(1 - a) \tag{3.2}$$

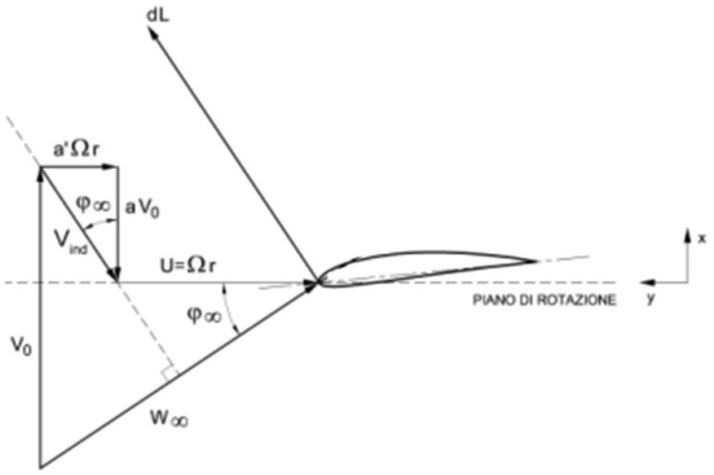

Figure 3.4: Glauert's 1D model

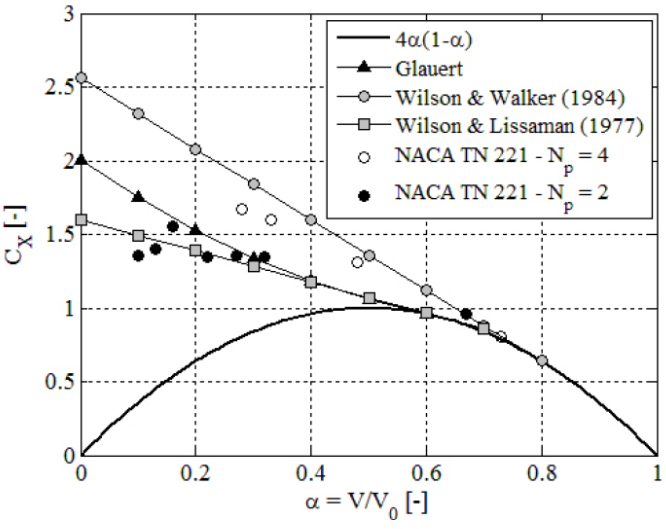

Figure 3.5: Some possible corrections that can be applied at Glauert's model.

$$F = \frac{2}{\pi}\arccos(e^{-f}) \tag{3.3}$$

$$f = \frac{N_b}{2}\frac{R-r}{r*\sin(\phi)} \tag{3.4}$$

$$\phi = atan(\frac{(1-a)}{(1+a')x} \tag{3.5}$$

The expression (3.5) has to be used instead of the (3.1) because drag has to be considered to draw the shape of the velocity triangle and the simple situation of Figure (3.4) with $\phi = \tan(a/a')$ is no more valid.
Once that a, a' and ϕ are known the velocity triangle is defined (considering also known the tangential velocity U of the blade) so also the relative velocity W can be evaluated.
It should be now the time to evaluate Re, but other parameters are unknown. In fact the entire BEM process is implicit and some "*first guess*" values have to be assumed to start the algorithm represented in Figure (3.6). Equation () 3.4) introduces a problem in the definition of the tip radial coordinate. In fact, when $r = R$, f becomes 0 and so does F. This is counter intuitive because the tip region is the one that should produce more power (because of it's higher speed) and so is important not to neglect it. On the other side, the tip is affected by 3D effects like vortex generation (due to the finite blade length), causing losses.
We found $r_{tip} = 0.96$ as a good value for compromise.

The solidity $\sigma = cN_b/2r\pi$ can be expressed as in (3.6). Than other quantities have to be evaluated from databases. The double-loop control is on residuals of a and a' respect to the previous step.
Once the solution has been found for each of the reference profiles (at hub, primary and tip), the performances[4] have to be interpolated on the entire blade.

$$\sigma = \frac{(4Fa*\sin(\phi)\tan(\phi)/(1-a))}{1+C_d*tan(\phi)/Cl}\frac{1}{C_l} \tag{3.6}$$

3.3 After the BEM algorithm

The interpolation uses basically the same relations showed before considering a and a' from Glauert's table to maintain an optimal distribution. The

[4]Not the geometry

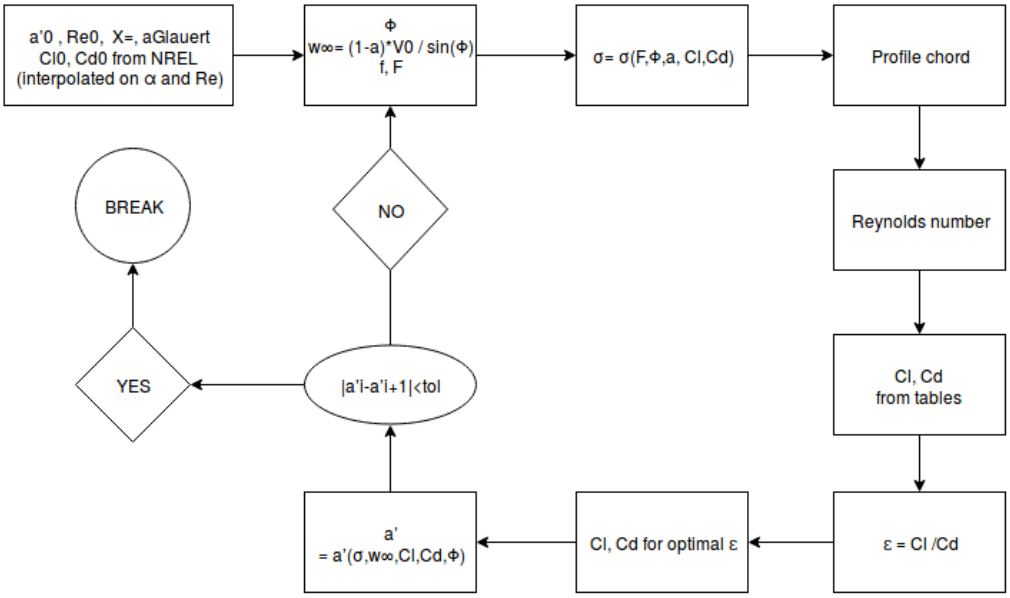

Figure 3.6: First iterative algorithm

structure can be recognised in this part of code[5]:

```
%% Opt chord - BLADESPAN
[CL,CD]=blade(...) % loading from database
EFF=CL./CD;
BETAinf=ones(1,length(r));
sigma=BETAinf;
corda=BETAinf;
for i=1:length(r)
    BETAinf(i)=alfa(EFF(:,i)==max(EFF(:,i)));
end
a_pi=a_p;
for i=1:length(r)
    a_pold=1;
    while abs(a_pi(i)-a_pold)>tol
        a_pold=a_pi(i); % a from Glauert
        phi(i)=atan((1-a(i))/((1+a_pi(i))*x(i)));
        W(i)=(1-a(i))*V0/sin(phi(i));
        f(i)=Nb*(R-r(i)*R)/(2*r(i)*R*sin(phi(i)));
        F(i)=2/pi*acos(exp(-f(i)));
```

[5] *Matlab*®

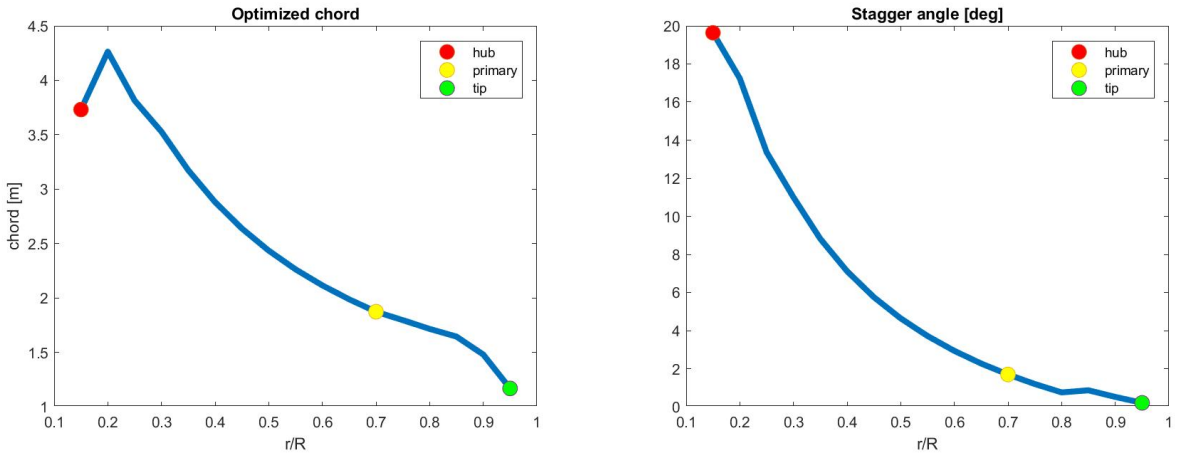

Figure 3.7: Optimal chord (*right*) and stagger angle (*left*) as function of the radial coordinate.

```
        Cl(i)=CL(EFF(:,i)==max(EFF(:,i)),i);
        Cd(i)=CD(EFF(:,i)==max...
        sigma(i)=((4*F(i)*a(i)*sin(phi(i))*tan(phi(i))/(1-a(i)...
        corda(i)=sigma(i)*2*pi*r(i)*R/Nb;
        a_pi(i)=sigma(i)*W(i)*(Cl(i)-Cd(i)/tan(phi(i)))/(4*omega...
    end
end
```

The results of this first part of the project are the distributions of the chord length and of the stagger angle $\beta_c = \phi - \beta_\infty$ shown in Figure 3.8.

Real blade will never have such a complex shape because of manufacturing costs and structural reasons. What is usually done is to linearise the change of the chord along the span. A structural limit that was suggested was to limit the maximum chord to the value of $0.12 * R = 4.11\ m$.
In Figure 3.8 is possible to see two examples.

Now the problem is that we have imposed a new shape to the blade, which can be seen in Figure 3.9 and so all the aerodynamic properties have to be evaluated once again with a procedure that is somehow the inverse with respect to the previous one as can be seen in Figure 3.10.
Again we have to do this for hub, primary and tip.

Than we interpolate aerodynamic properties again along the blade as seen before except for the fact that we are no more respecting Glauert's distribution and so also a *while-loop* for a is needed.

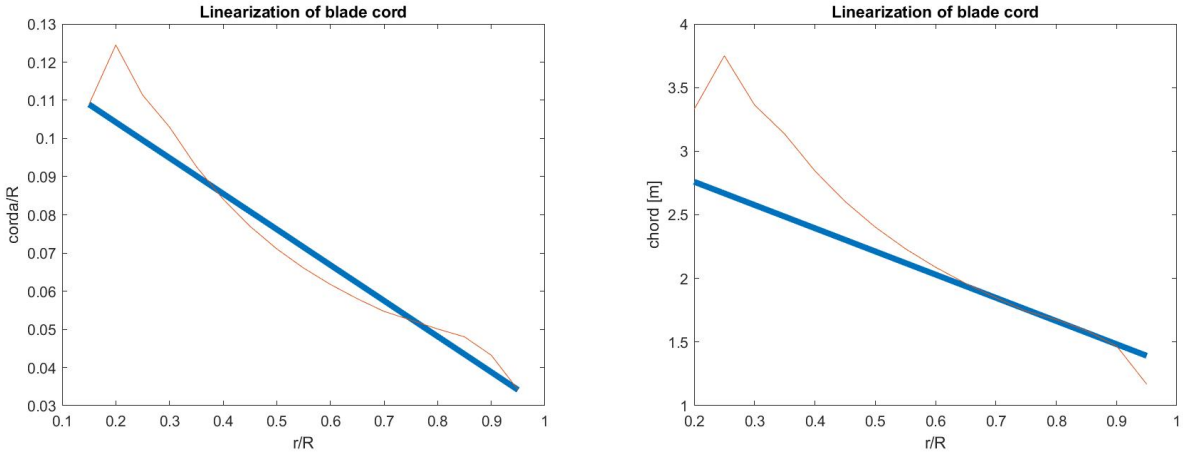

Figure 3.8: Suggested linearisation (*right*) and our choice (*left*) that optimises better the C_p of the entire blade.

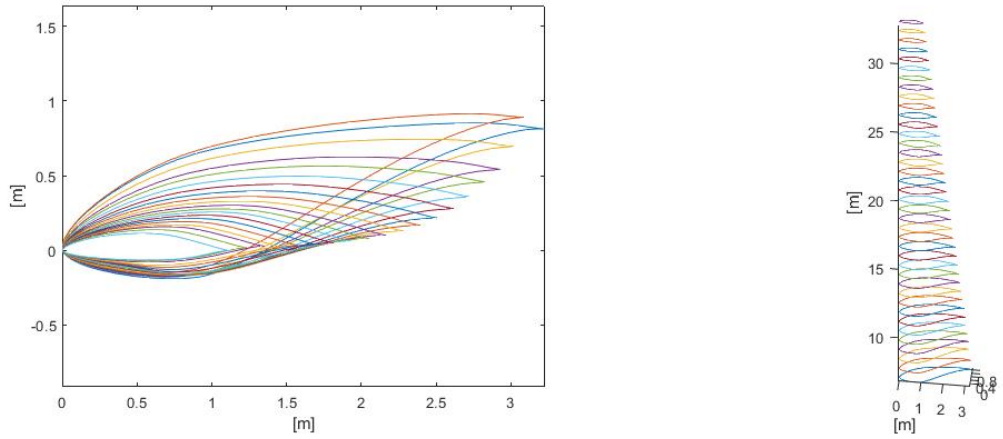

Figure 3.9: Two views of the profile variations. Pay attention that this is not the final blade shape because profiles are not aligned along the leading edge but respect the centre of aerodynamic forcing.

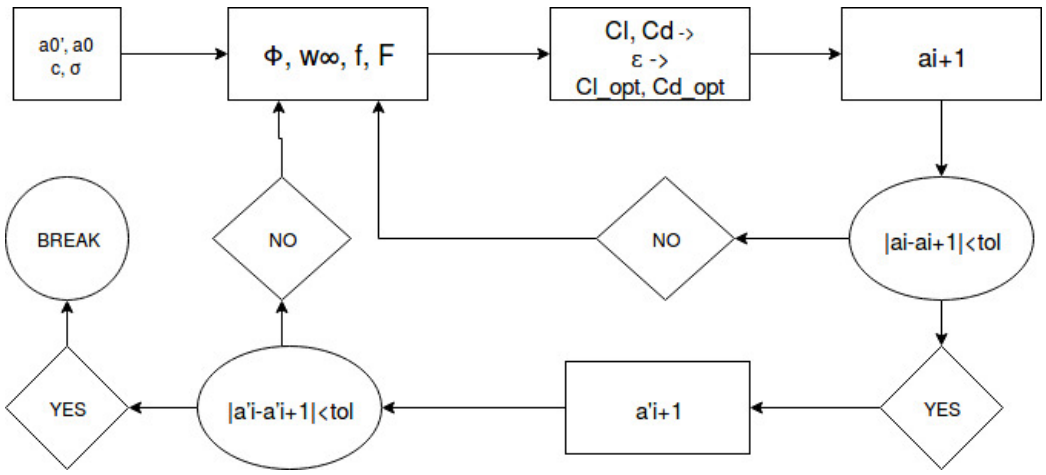

Figure 3.10: Second iterative algorithm

3.4 Results and performances

Eventually, it is possible to evaluate the design performances of the blade. The global power coefficient (and so the power) can be found both from a balance of aerodynamic forces and from a momentum balance. Having two ways of evaluation is useful to compare results.
The force balance gave as a result $P_{FB} = 775.99kW$ while the momentum balance gave as a result $P_{MB} = 776.31kW$, so P_d of our turbine is $776KW$. Considering the Re effect the result is $768.9kW$, so just the 0.99% less. This because Re is so high that the flow can be considered fully turbulent, thus the behaviour of the turbine is independent from it.
This result can be divided by the area swept by the blades [6] to obtain the *Specific Rated Output* (**SRO**) of the turbine can be calculated. In our case it is SRO=0.48, in accordance with statistical data of similar turbines (also considering the wind class around 8.5 m/s).

[6] *Area Disk* $(A_D) = R^2\pi = 3.683m^2$

Chapter 4

Off-design assessment

The off-design of a wind turbine consists basically in the study of the change in performance that affect it caused by a wind speed different from the design one and, subsequently, the control to apply to extract as much power as possible at low wind speed and keep it as constant as possible at high speed. The control of an HAWT can be performed with a combination of rotation speed and blade pitch variation. Usually they are both possible on large size machines like our because the cost and the required complexity are justified by the huge building and maintenance price of such machines.
Basically the procedure consist in repeat all the aerodynamic assessment on the blade seen in the design part for each considered wind speed.

4.1 First range - variable speed

The first range of application is between the so called *velocity of cut-in* (V_{cut-in}), velocity at wich the turbine starts to rotate, and V_C, at witch the turbine reaches the maximum rotating speed. On this interval the aim is to control the rotating speed in a way to keep λ constant.
In our case we choose a $V_{cut-in} = 3.5\ m/s$ (justified by our machine size) and a $V_C = 9\ m/s$.
Given the λ_{design} and known the considered wind speed is also known the rotation speed of the turbine. This allows to evaluate the velocity triangle, while the knowledge of the blade geometry allows to evaluate Re and than C_L and C_D. From the momentum equation a and a' can be evaluated and than is possible to start an iteration.

```
%% RANGE A-C
omega=ones(1,length(vAC));
```

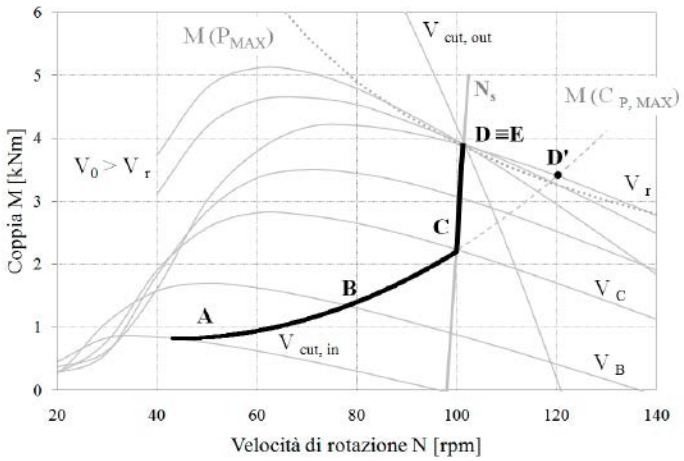

Figure 4.1: The black line show the control strategy of a variable-pitch/variable-speed wind turbine.

```
CpAC=omega;PowerAC=omega;CpAC2=CpAC;PowerAC2=PowerAC;

for j=1:length(vAC)
    omega(j) = lambda_d*vAC(j)/R;
    xACj = (omega(j)*(r*R)/vAC(j))
    x_h = xACj(r==r_H); x_p = xACj(r==r_P); x_t = xACj(r==r_T);
    %% a-c: H,P,T
    %hub
    ah=ad(r==r_H); .... % first step quantities
    while abs(aph-apold)>tol
        apold=aph;
        while abs(ah-aold)>tol
            aold=ah;
            phi=atan((1-ah)/((1+aph)*x_h));
            w=(1-ah)*vAC(j)/sin(phi);
            f=Nb*(R-r_H*R)/(2*r_H*R*sin(phi));
            F=2/pi*acos(exp(-f));
            Reh=w*cordalin(xACj==x_h)/ni;
                if Reh<=1e6 % control on Re
                ...
                end
            medh=Re_medio(hub1(1,:)... % data interpolation
            ah=sol(xACj==x_h)*w*(medh(1,alfa==BETAinf(r==r_H))/...
            ah=e*ah+(1-e)*aold;
```

```
    end
    aph=sol(xACj==x_h)*w*(medh(1,alfa==BETAinf(r==r_H))...
    aph=e*aph+(1-e)*apold;
end

%primary
...
%tip
...

%% a-c: BLADESPAN
% blade distribution of cl and cd
[cl,cd]=blade(... % data
% calculation of a and a' for all blade's parts
aAC=ones(1,length(r));
n=aAC;apAC=aAC;n2=aAC;
for i=1:length(r)
    aAC(i)=ad(i); ... % first step data
    while abs(apAC(i)-apold)>tol
        apold=apAC(i);
        while abs(aAC(i)-aold)>tol
            aold=aAC(i);
            n2(i)=n2(i)+1;
            phi(i)=atan((1-aAC(i))/((1+apAC(i))*xACj(i)));
            w(i)=(1-aAC(i))*vAC(j)/sin(phi(i));
            f=Nb*(R-r(i)*R)/(2*r(i)*R*sin(phi(i)));
            F_AC(i)=2/pi*acos(exp(-f));
            aAC(i)=sol(i)*w(i)*(cl(alfa==BETAinf(r==r(i)),i)...
            aAC(i)=e*aAC(i)+(1-e)*aold;
        end
        apAC(i)=sol(i)*w(i)*(cl(alfa==BETAinf(r==r(i)),i)...
        apAC(i)=e*apAC(i)+(1-e)*apold; % "e" is for eq. relaxation
    end
end

% Power and Cp calculation
...
```

4.2 Second range - variable pitch to avoid stall

After the maximum rotating speed is reached the aerodynamic of the turbine can be adapted varying the pitch of the blade up to the V_{rated} (or V_r), that is the speed at the turbine produces the rated power. This power is different from the design one because, while the design considers the average wind speed, the rated is reached for an higher wind speed for a lower amount of time. The best value of trade-off (between rarity of such a speed and performance improvement) can be found in literature [1] and for us was 15 m/s.
Without plotting again the code or the procedure, it is sufficient to say that, varying the $beta_c$ of the blade, it is necessary to avoid the stall condition. Knowing the profiles properties from database and the distribution of profiles along the blade, is possible to define a "reference stall condition" when the efficiency of the profile (so the ratio C_L/C_D) in lower than the 95% of the optimal one. We put the limit condition on a stall involving the 20% of the blade.

4.3 Third range - variable pitch to feather

The last part of the range is between the V_r and the $V_{cut-off}$, that is the maximum wind speed that the machine can afford before being stopped for safety reasons. In this range the rated power is reached and so the turbine can no longer extract all the ideal power available from the wind. The target is to maintain the extracted power as constant as possible varying β_c (without stall limits). So the previous procedure is again repeated with the iteration control no more on the percentage of stalled profiles but on the error on the produced power, that is $|P - P_r| < tollerance$.

4.4 Results

In Figure 4.2 it is possible to see the variation of produced power and power coefficient as function of the wind speed. the control strategy can be summarized in the following way: at the beginning the target is to operate at maximum efficiency to extract as much power as possible from a wind flow that has a low power content. Than the aerodynamic of the blade is changed through the pitch rotation and so C_P decreases. In the last part the power

[1] Wind Energy Handbook - J.W. and sons, 2001

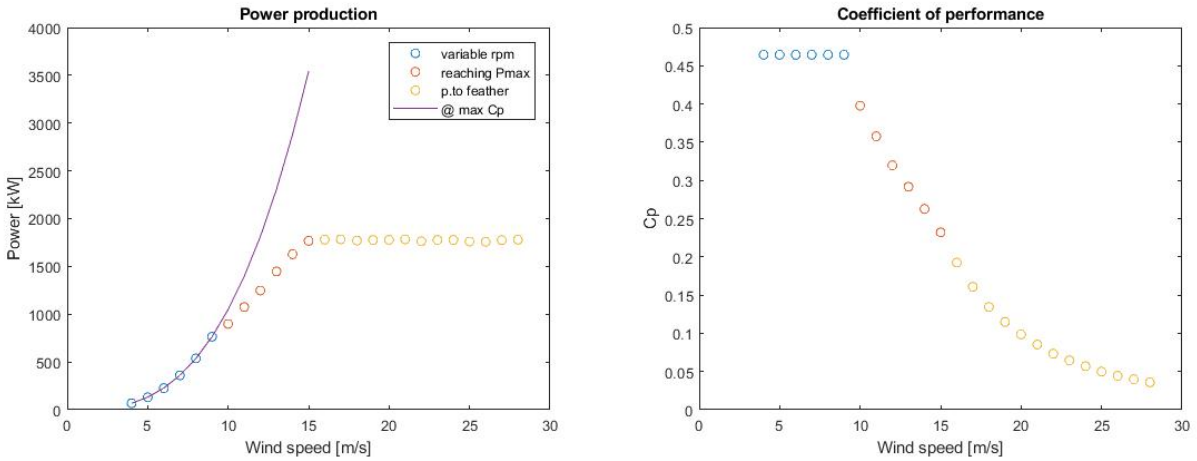

Figure 4.2: Power (*left*) and C_P (*rigth*) as functions of the wind speed

.

contained in the wind continue to grow while the extracted power remains constant. This brings to a decay in the power coefficient.

4.5 Critical issues

The range of α at which profiles are operated on HAWT is much wider than in wings or air-foils, so the data available in common databases have to be extended in the stall region (hiag values of α) and also for low and negative α. Fot the stall region the Viterna-Corrigan correlation [2] is used, while for the previous region a first approximation is obtained just mirroring the C_L and C_D behaviour between $\alpha = 0$ and beginning of stall to make it symmetrical respect to $(\alpha(C_L = 0), C_L = 0)$ as can be seen in Figure 4.4.

[2]Viterna, L .A., and Corrigan, R. D., "Fixed Pitch Rotor Performance of Large Horizontal Axis Wind Turbines," DOE/NASA Workshop on Large Horizontal Axis Wind Turbines, Cleveland, Ohio, July 1981

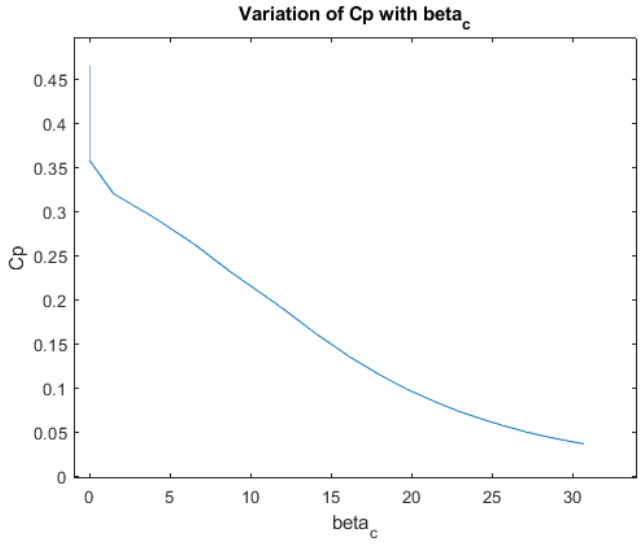

Figure 4.3: Variation of C_P as function of β. The first vertical part of the plot represente the speed-control range.

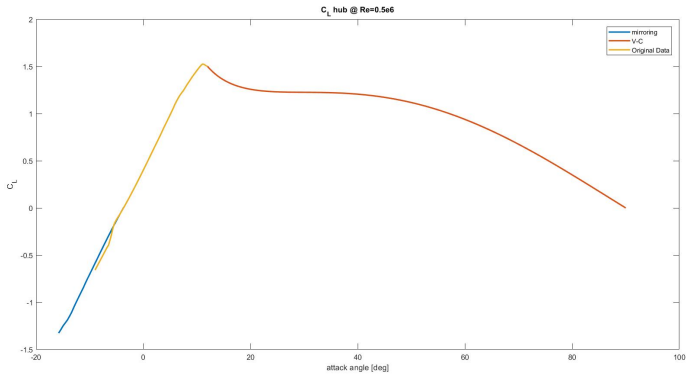

Figure 4.4: Example data extension for the C_L on the entire range of aplication.

Chapter 5

Modal Analysis with a 1-D Finite Element Model

Like all rotative machines, wind turbines are subjected at alternate loads that causes vibrations. We decided to see how would be possible to set a preliminary model to study the vibration of our 80m [1] tall turbine.

5.1 The model

The *Finite Element Method* (**FEM**) [2] is a mathematical tool used to study the behaviour of complex systems through their decomposition in a certain number of simpler subparts. The behaviour of the entire system is considered approximated by the sum of the behaviours of all the subparts.
In our case subparts are so-called "beam elements", which means they have a longitudinal dimension much more relevant respect to the others. Each beam element is a segment (so 1D) on which are concentrated all the geometrical and physical characteristic of the real structural or mechanical part. Working in a plane, these elements have 6 *degrees of freedom* (**DoF**), as can be seen in Figure 5.1.

Inertia, stiffness and damping of the system can be synthesized assembling $\boldsymbol{M}$, $\boldsymbol{K}$ and $\boldsymbol{D}$ matrix of each beam. This produces a system of equation represented by $[M]\ddot{\bar{x}} + [D]\dot{\bar{x}} + [K]\bar{x} = \bar{F}$, where $\bar{x}$ is the vector of DoF and $\bar{F}$ the vector of external forces applied in each DoF.

[1] From literature is common practice to have $H = \frac{3}{2}D$, where H is the pillar height.
[2] Advanced Dynamics of Mechanical Systems - F. Cheli, G. Diana; Springer (2005)

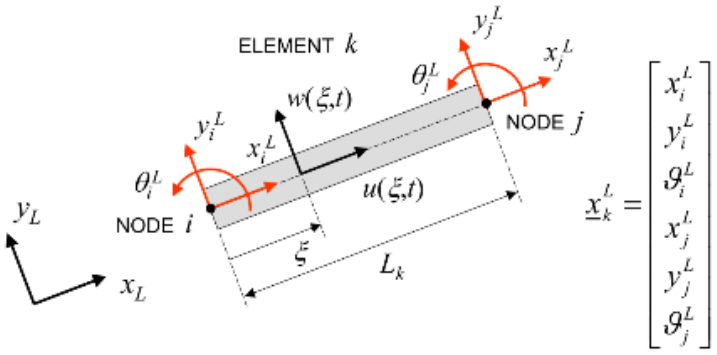

Figure 5.1: The model of a beam element with its 6 DoF.

$$[M_k^L] = \begin{bmatrix} \frac{1}{3}mL_k & 0 & 0 & \frac{1}{6}mL_k & 0 & 0 \\ 0 & \frac{13}{35}mL_k & \frac{11}{210}mL_k^2 & 0 & \frac{9}{70}mL_k & -\frac{13}{420}mL_k^2 \\ 0 & \frac{11}{210}mL_k^2 & \frac{1}{105}mL_k^3 & 0 & \frac{13}{420}mL_k^2 & -\frac{1}{140}mL_k^3 \\ \frac{1}{6}mL_k & 0 & 0 & \frac{1}{3}mL_k & 0 & 0 \\ 0 & \frac{9}{70}mL_k & \frac{13}{420}mL_k^2 & 0 & \frac{13}{35}mL_k & -\frac{11}{210}mL_k^2 \\ 0 & -\frac{13}{420}mL_k^2 & -\frac{1}{140}mL_k^3 & 0 & -\frac{11}{210}mL_k^2 & \frac{1}{105}mL_k^3 \end{bmatrix} \quad [K_k^L] = \begin{bmatrix} \frac{1}{L_k}EA & 0 & 0 & -\frac{1}{L_k}EA & 0 & 0 \\ 0 & \frac{12}{L_k^3}EJ & \frac{6}{L_k^2}EJ & 0 & -\frac{12}{L_k^3}EJ & \frac{6}{L_k^2}EJ \\ 0 & \frac{6}{L_k^2}EJ & \frac{4}{L_k}EJ & 0 & -\frac{6}{L_k^2}EJ & \frac{2}{L_k}EJ \\ -\frac{1}{L_k}EA & 0 & 0 & \frac{1}{L_k}EA & 0 & 0 \\ 0 & -\frac{12}{L_k^3}EJ & -\frac{6}{L_k^2}EJ & 0 & \frac{12}{L_k^3}EJ & -\frac{6}{L_k^2}EJ \\ 0 & \frac{6}{L_k^2}EJ & \frac{2}{L_k}EJ & 0 & -\frac{6}{L_k^2}EJ & \frac{4}{L_k}EJ \end{bmatrix}$$

Figure 5.2: M (*left*) and K (*rigth*) matrix for a beam element

.

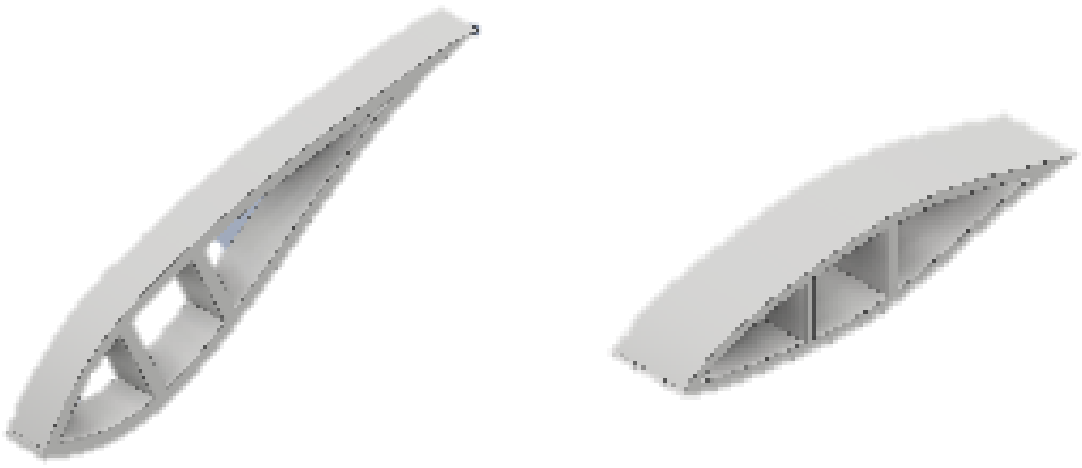

Figure 5.3: Blade elements shown with their internal structure.

.

Table 5.1: Structural analysis recap

PILLAR			**NACELLE+ROTOR**		
s	0,0458	m	h	3	m
Safety c.	5		b	3	m
S355	7850	kg/m3	l	15	m
H	80	m	Rot. inerzia	1,5	m^4
Thrust	142,3406	kN	vol	135	m3
D_ext	3	m	rho	570,37	kg/m3
$rotor_m$	28	ton	Nac. inertia	855,55	kg*m
$nacelle_m$	49	ton	Nac. mass	77000	kg
$tower_m$	267,47	ton	Jxx	0,464	m^4
$blade_m$	4,5	ton	σ_comp	8,245	MPa
tot_m	3511,76	kN	σ_f	36,754	MPa
Pill. mass	3343,47	kg/m	σ_max	45	MPa
Pill. inertia	0,4647	m^4	Pill. section area	0,2146	m^2

To obtain geometrical quantities to model the blade we used the CAD software *Inventor*® and the geometry obtained in Section 3.3. For the physical quantities (like density and Young modulus) we used a weighted average considering the percentage of each material that is used in the structure (95% glass reinforced plastic and 5% steel for the blade and 98% steel and 2%concrete for the tower [3] [4]). This is done because our study was focused only on the aerodynamic design of the blade without considering all the complex structural and manufacturing needs that can be shown in Figure 5.4 where each colour represents a different material. For the mass of the nacelle (modelled as a concentrated mass) we looked at similar turbines and than we choose a mass of 77000 kg.
To dimension the pillar a structural analysis was required. Having computed principal loads, hypothesized relevant masses and chosen the the material, with an iterative cycle on *Excel*® was possible to estimate the thickness of the pillar (i.e. the section area as can be seen in Table 5.1).

Each element of each matrix is referred to a precise DoF of the complete system. To identify the natural frequencies of the system is needed to evaluate the eigenvalues of the system considered only with $[M_{FF}]$ and $[K_{FF}]$, where FF indicates only the elements relative to the non-constrained DoF.

[3] Wind Turbine - Materials and Manufacturing Fact Sheet http://citeseerx.ist.psu.edu
[4] Aerodynamic and Structural Integrated Optimization Design of Horizontal-Axis Wind Turbine Blades

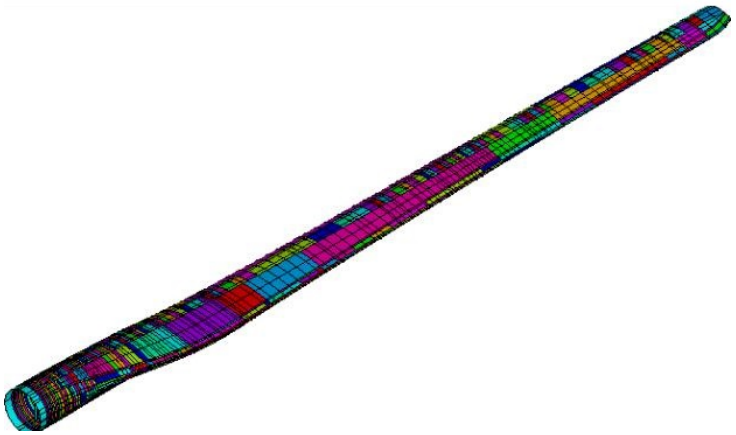

Figure 5.4: Internal structure of a real blade with highlight of material distribution.

Once the natural frequencies are known (and they are as many as the considered DoF, so theoretically infinite in reality) it is possible to evaluate the "mode shape", that are the ways (non-dimensional) in which the structure vibrate. The first thing that can be noticed is that natural frequencies involving the tower are much lower than blades one. Those frequencies are slightly coupled due to the very low damping of the structure [5].

5.2 Results

First of all we have to say that, with the increase of the frequency, the amplitude of the oscillations decreases (so the correspondent vibration mode is less relevant). That is why it is not necessary to evaluate all the natural frequencies of the model. However, the fact that the pillar (that can be seen as a very stiff reverse pendulum because of the nacelle) and blades have natural frequencies with two order of magnitude of difference (from 1Hz to 0.1kHz), makes necessary to go more in detail also at high frequencies.

Also considering the various approximations that such a model implies, we can use this approach to identify some possible range of risk for our structure. In fact we can compare natural frequencies of the system with the ones of external forcing (for example earthquakes or waves for off-shore applications), but also (and more important) with natural frequencies of internal

[5] It is not considered in the evaluation of natural frequency, but from experimental measures we know that it can be considered very low (in fact in some cases at the base of some HAWT is possible to find hydraulic dampers to compensate this problem): from 3% to 6,3% respect to the modal mass for the DTU10MW

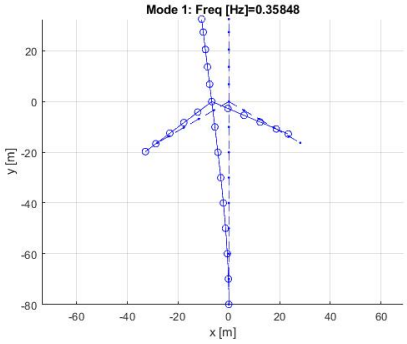

(a) 1st vibration mode

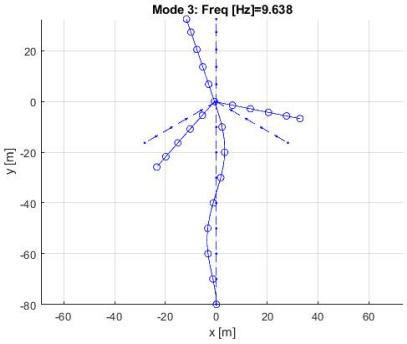

(b) 3rd vibration mode

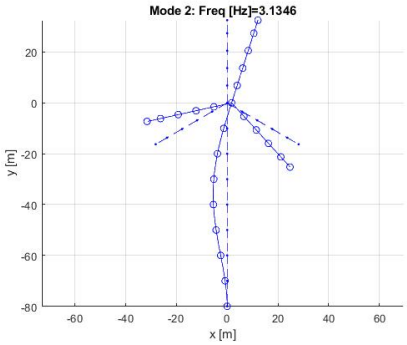

(a) 2nd vibration mode

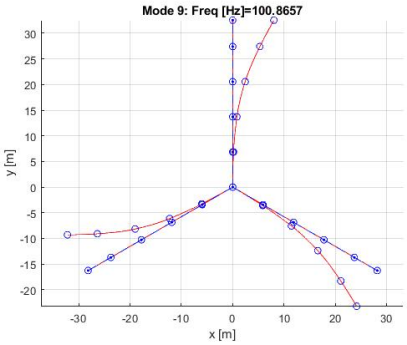

(b) 3rd blade vibration mode

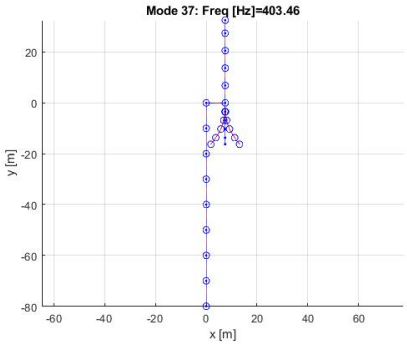

(a) Counter phase vibration of blades

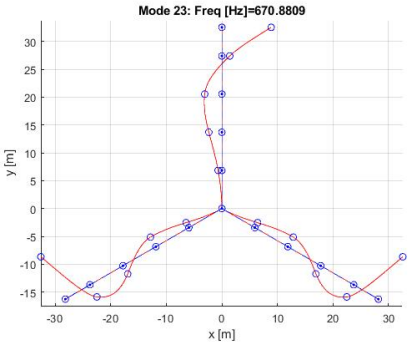

(b) 8th blade vibration mode

Figure 5.5: Examples of results

components like transmission elements, electrical generator, ball bearings etc. Anyway the most important forcing acting on a HAWT has a frequency of $N_b\omega$, that is the frequency of the passage of a blade in front of the tower,

which causes the impact of the blade-wake with the tower itself.

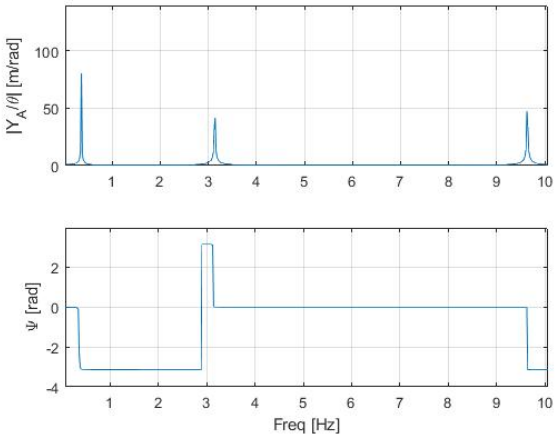

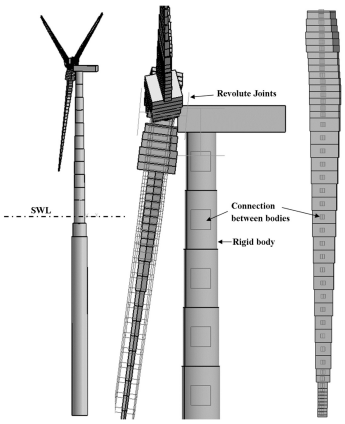

(a) Frequency response function to a displacement of the tower base (like in a earthquake). The first plot shows the amplitude and the second one the phase of the oscillation.

Figure 5.6

$mode$	$Frontview[Hz]$	$Sideview[Hz]$	$Bladesfrontview[Hz]$	$Bladessideview[Hz]$
1	$0,358$	$0,302$	$44,901$	$44,901$
2	$3,134$	$2,993$	$92,411$	$89,802$
3	$9,638$	$8,332$	$100,86$	$92,411$
4	$10,50$	$9,753$	$155,36$	$100,87$
5	$19,80$	$17,75$	$229,57$	$155,36$

The *blade passing frequency* (**BPF**) is function of the rotation speed and so is variable in the first range of wind speed in which the turbine is operating. In our case the range of rotating speed is between 0.817 and 1.840 $[rad]/s$, that means a range of frequencies between 15.41 Hz and 34.67 Hz. So at least the first 4 modes of the machine are in a safe region.
Another relevant frequency is the one of the electrical generator that is $2f_{grid} = 100Hz$. This correspond to the 3rd natural frequency of the blade.

5.3 Conclusions

The BPF is not so warning, usually are considered the first 3-4 modes as the ones with higher amplitude if stimulated.
The electromechanical coupling can't be avoided, so the blades needs a dif-

	Ball bearing	Taper roller bearing
Inner race roller passing frequency (f_{rpi})	$\frac{n(f_o - f_i)(1 + (RD/PD)\cos\alpha)}{2}$	$n(f_o - f_i)\frac{OD}{OD + ID}$
Outer race roller passing frequency (f_{rpo})	$\frac{n(f_o - f_i)(1 - (RD/PD)\cos\alpha)}{2}$	$n(f_o - f_i)\frac{ID}{OD + ID}$
Cage rotating frequency (f_c)	$\frac{f_i(1 - (RD/PD)\cos\alpha)}{2} + \frac{f_o(1 + (RD/PD)\cos\alpha)}{2}$	$\frac{f_i \times ID + f_o \times OD}{OD + ID}$
Roller spinning frequency (f_{rs})	$\frac{(f_o - f_i)}{2}\frac{PD}{RD}(1 - ((RD/PD)\cos\alpha)^2)$	$(f_o - f_i)\frac{ID}{RD}\frac{OD}{OD + ID}$

n = number of rollers, f_o = outer race rotating speed (rps), f_i = inner race rotating speed (rps), OD = outer race diameter, ID = inner race diameter, RD = roller diameter, PD = pitch circle diameter, α = contact angle.
These equations were derived under the assumption that it is pure rolling contact (no slipping, skidding, etc.) and perfect geometry even under load. One would expect some deviations under actual conditions.

Figure 5.7: Evaluation of bearing passing frequencies

ferent design in therms of geometry and materials.
With this preliminary and very low time consuming analysis a first design hypothesis of the internal elements can be made. For example, the *Gear Mesh Frequency* (**GMF**) of the gearbox depends, for each reduction stage, on axis *rps* and N_{teeth}, while for roller bearings some formulas are shown in Figure (5.7) [6].
Of course a deeper analysis with a CAE software is necessary, but it is also more computationally expensive.
An implementation of this model can be done with a different model of the foundations, with lumped elements in function of the location ground. An example of the complexity that such a methodology can reach is reported in Figure 5.6 on the right [7].

In the last page we provide some extra plots with additional results.

[6] From the course "097552 - Rotordynamics and diagnostics" of Prof. P.Pennacchi, A.Y.17-18"

[7] Coupled multi-body dynamics and CFD for wind turbine simulation including explicit wind turbulence - Y. Li, A.M. Castro, T. Sinokrot, W. Prescott, P.M. Carrica

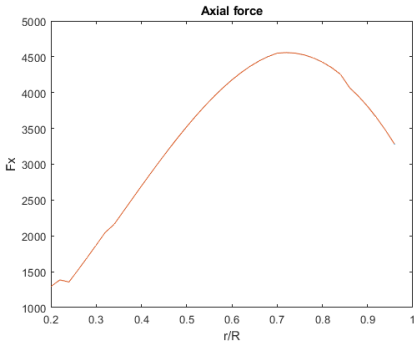
Axial force
Fx
r/R

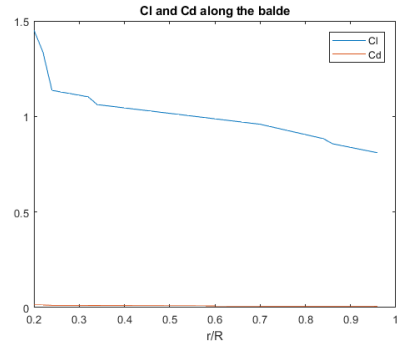
Cl and Cd along the balde
Cl
Cd
r/R

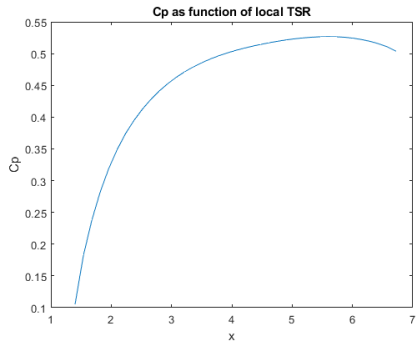
Cp as function of local TSR
Cp
x

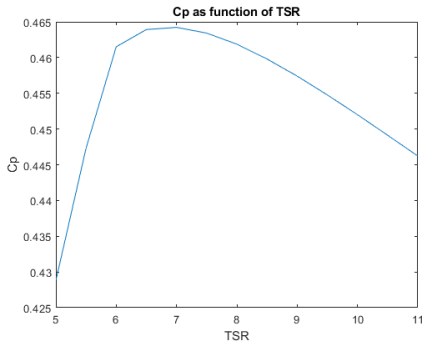
Cp as function of TSR
Cp
TSR

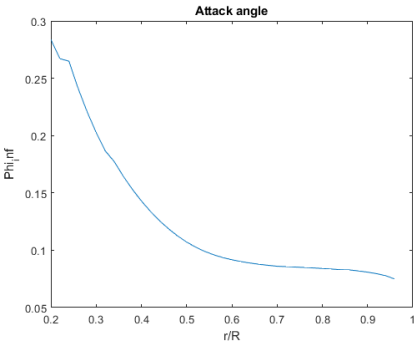
Attack angle
Phi_inf
r/R

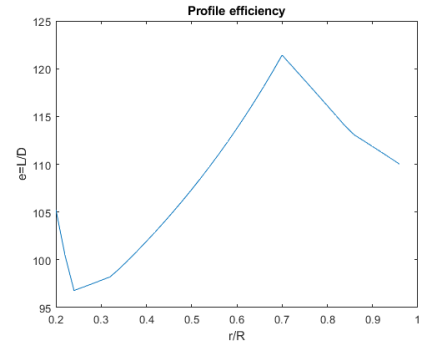
Profile efficiency
e=L/D
r/R

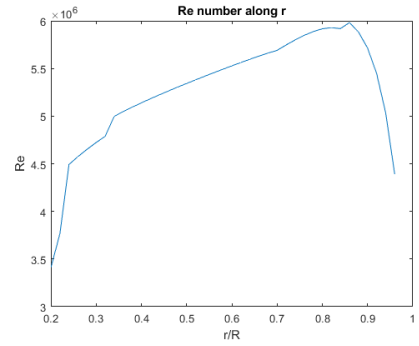
Re number along r
Re
r/R

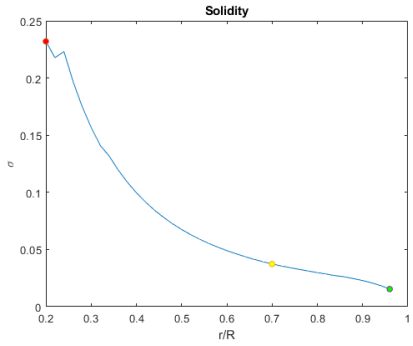
Solidity
σ
r/R